Nanoscale crystal fabric of primary Ediacaran dolomite

Julia Wilcots[1], Pupa U. P. A. Gilbert[2], Kristin D. Bergmann[1]

[1]Department of Earth, Atmospheric and Planetary Sciences, Massachusetts Institute of Technology, Cambridge, MA

[2]Departments of Physics, Chemistry, Materials Science, Geoscience, University of Wisconsin, Madison, WI

Key Points:

- High-resolution imaging of a 574 Ma dolomite ooid reveals a novel crystal fabric and informs our understanding of the "dolomite problem."
- The ooid is comprised of very fine dolomite crystals arranged in plumose spherulitic bundles.
- We interpret this ooid formed via primary dolomite precipitation at the onset of the Shuram carbon isotope excursion.

Corresponding author: Julia Wilcots, jwilcots@mit.edu

Abstract

Dolomite ($CaMg(CO_3)_2$) forms in minor quantities in few modern environments yet comprises most of the Precambrian carbonate rock record. Precambrian dolomites are often fine-grained and fabric-retentive and are interpreted to have precipitated as primary cements or formed as early diagenetic replacements of $CaCO_3$. Primary dolomite precipitation from seawater in depositional environments has not yet been described. Here, we use synchrotron radiation to produce a nanoscale-resolution crystal orientation map of one exquisitely preserved ooid deposited at the onset of the Shuram carbon isotope excursion at ∼574 Ma. The crystal orientation map reveals small (∼10 μm) acicular, radially-oriented crystals grouped into bundles of similarly-oriented crystals with varying optical properties. We interpret this dolomite formed via primary, spherulitic precipitation during ooid growth in shallow marine waters. This result provides additional evidence that the physicochemical properties of late Precambrian oceans promoted dolomite precipitation and supports a primary origin for the Shuram excursion.

Plain Language Summary

The mineral dolomite is a common constituent of ancient carbonate sedimentary rocks, yet dolomite rarely precipitates from seawater today. For decades, this discrepancy has caused researchers to wonder whether dolomite precipitated directly from seawater in the deep past. If so, dolomitic rocks — like other carbonate sedimentary rocks — could preserve the physical and chemical properties of the water from which they formed and serve as a record of ancient marine conditions. However, evidence for primary dolomite precipitation from seawater has not been described. Here, we apply a new method and study one 574 million-year-old dolomite at nanometer resolution using x-ray light, creating a three-dimensional map of crystals in this sample. We discover our sample is comprised of tiny, needle-shaped dolomite crystals that are arranged in bundles of similarly-oriented crystals — a novel crystal fabric. After comparison to modern primary and lab-grown dolomites and to other ancient dolomites, we interpret this crystal fabric to have formed via precipitation from seawater. Our discovery of a new dolomite crystal fabric and our interpretation that it precipitated from seawater shed new light on the ancient environment in which this sample formed.

1 Introduction

Carbonate rocks serve as the primary sink for carbon in the Earth system and preserve a record of the physical, chemical, and biological properties of marine settings throughout geologic time. The geological interpretation of carbonates through Earth history elucidate

past changes in climate and carbon cycling, and also provide insight into potential future changes to the Earth system.

In Precambrian (>541 Ma) strata, carbonates are predominantly comprised of dolomite (Cantine et al., 2020), and petrographic observations of these ancient dolomites commonly reveal fine, detail-preserving, and mimetic (fabric-retentive) crystal fabric (Corsetti et al., 2006; Hood et al., 2011; Hood & Wallace, 2018; Tucker, 1982, 1983). Peculiarly, although modern seawater is supersaturated with respect to dolomite, aragonite ($CaCO_3$), not dolomite, is the carbonate mineral precipitated abiotically on modern marine shelves; dolomite can only be found forming on Earth's surface today in unique hypersaline, hydrothermal, lacustrine, or biologically-mediated environments. The origin of Precambrian fabric-retentive dolomites and dearth of modern analogues has puzzled researchers for many decades — solving this "dolomite problem" would greatly advance our understanding of Earth during Precambrian time.

The finely crystalline petrographic fabrics common in Precambrian dolomites have been used as evidence to suggest that much of the Precambrian dolomite preserved in shallow-water carbonate successions formed in early diagenetic settings from seawater-like fluids (Hood et al., 2011; Knoll & Swett, 1990). Early diagenetic, fabric-retentive dolomite is difficult to define mechanistically because many of the processes governing dolomite formation in shallow subsurface or surface-like settings are poorly constrained. Understanding how early diagenetic dolomite formed and whether it can be used as a faithful geochemical recorder of ancient seawater chemistry is crucial in the quest to reconstruct Precambrian environments.

The pursuit to explain fabric-retentive early diagenetic dolomite and thus better understand the Precambrian world has inspired the exploration of many mimetic dolomites of late Precambrian and early Paleozoic age. Petrographic evidence has been used to show that primary dolomite cements precipitated in pore space and cracks in Neoproterozoic-aged (1000-541 Ma) reefs (Hood et al., 2011; Hood & Wallace, 2018; Tucker, 1983), to interpret (Corsetti et al., 2006) and model (Zempolich & Baker, 1993) the mimetic replacement of aragonite by dolomite, and to suggest that Neoproterozoic fabric-retentive dolomites may have precipitated directly from seawater, instead of replacing original calcite or aragonite (Tucker, 1982). Early-forming dolomite appears more common in the late Precambrian, suggesting these Neoproterozoic seas had exceptional early (or primary) dolomite-forming potential.

Many prior petrographic studies have relied on ooids – spherical carbonate grains that form via precipitation from solution in high-energy shallow marine environments – as reliable

petrographic indicators of primary mineralogy (Corsetti et al., 2006; Hood & Wallace, 2018; Sandberg, 1975; Tucker, 1982). Ooid mineralogies are nearly always interpreted as primary aragonite or calcite, not as primary dolomite. However, in some cases (most frequently in the Precambrian and particularly in the Neoproterozoic succession of Death Valley, USA), ooid fabrics are so pristinely preserved in dolomite that researches have pondered whether they could represent primary dolomite precipitation (Corsetti et al., 2006; Tucker, 1982).

Here, we study one such exquisitely preserved dolomitic ooid sampled from the ca. 574 Ma Khufai Formation (Sultanate of Oman). This grain was deposited in a widespread 1-30 m thick oolite at the onset of the Shuram excursion, the largest negative carbon isotope excursion in the rock record, found in Ediacaran-aged shallow marine successions (635-541 Ma) worldwide (Grotzinger et al., 2011). Numerous hypotheses have been put forward to explain the genesis of the Shuram excursion; arguments for both a secondary and primary origin have been proposed. A primary origin would likely require ∼synchronous enigmatic environmental conditions across shallow water carbonate platforms (e.g. Bergmann et al., 2011); a secondary origin would require a significant diagenetic event at Shuram time (e.g. Derry, 2010). Intriguingly, the dolomitic oolite bed of the Khufai Formation, studied here, shares petrographic and sedimentologic similarities with a widespread dolomitic oolite found at the base of the Shuram excursion in the Johnnie Formation (Death Valley, USA), see Figures 1 and 2 (Bergmann et al., 2011; Corsetti et al., 2006). Due to their commonly well-preserved crystal fabric, Johnnie Formation ooids have been interpreted as early diagenetic dolomitic replacement of primary aragonite (Corsetti et al., 2006), although they occur stratigraphically above similar ooids (of the Tonian Beck Spring Formation), that Tucker (1982) interpreted as primary dolomite.

Using synchrotron-based nanoscale crystal orientation mapping, electron probe micro-analysis (EPMA), and x-ray diffraction (XRD), we reveal the crystal morphology (size, shape, arrangement) and mineralogy of one ca. 574 Ma dolomitic ooid. We then interpret these observations in the context of previously proposed models of dolomite formation, prior petrographic studies of ooids, and the specific set of environmental conditions under which modern dolomite forms. We assess whether this ooid precipitated as an early diagenetic replacement of primary $CaCO_3$ or directly from seawater and discuss implications for the genesis of the Shuram excursion and properties of Precambrian shallow marine environments.

2 Formation models for fabric preserving dolomite

To establish a frame of reference in which to evaluate the fabric of our 574 Ma ooid, we characterize three models for the formation of fabric-retentive or primary dolomite from

literature, each differentiable on the basis of crystal morphology, optical characteristics, and mineralogy. **Mimetic replacement dolomite:** In laboratory conditions, modern aragonite ooids are replaced with euhedral, microsucrosic (2-8μm) dolomite crystals over 180 hours at 200°C (Zempolich & Baker, 1993). Rhombohedral dolomite crystals faithfully preserve tangential ooid macrostructure, but do not preserve primary optical characteristics (pseudo-uniaxial cross) (Zempolich & Baker, 1993). Notably, replacement begins on the outer surface of the ooid and progresses inward via micro pore spaces. **Precipitated primary dolomite:** Primary dolomite cements line pore spaces in Neoproterozoic carbonates (Hood & Wallace, 2018). Individual crystals have a variety of forms, but are generally fibrous or bladed in shape, form bundles that fan out from their nucleation site, have an invariably length-slow optical characteristic, and can grow up to ca. 2mm long (Hood et al., 2011; Hood & Wallace, 2018). **Precipitated primary protodolomite:** In laboratory conditions at high temperatures (60-200°C) and high dolomite supersaturation, protodolomite precipitates as nanocrystalline spherulites (Rodriguez-Blanco et al., 2015). The poorly ordered protodolomite precursor transforms to ordered dolomite comprised of larger (>100 nm), planar crystals over hours to days. Protodolomite forming in modern surface environments in close association with microbial communities can also be spherulitic (Vasconcelos et al., 1995).

3 Novel crystal structure of a ca. 574 Ma dolomite ooid

Recognizing the value of petrographic observations in the classification of ancient dolomites, we leverage the nanoscale resolution of synchrotron-based Polarization-dependent Imaging Contrast (PIC) mapping to produce a high-resolution map of crystal orientations and geometries within a ca. 574 Ma dolomitic ooid that appears exquisitely fabric-retentive in thin section (Fig. 2). Using soft x-rays with variable linear polarization angle, PIC mapping measures the c-axis orientations of nanocrystals and displays them in 3D, at 20nm resolution, using color: hue and brightness represent in- and out-of-plane angles, respectively (see A2 and Gilbert et al. (2011)). Since PIC mapping is based on x-ray linear dichroism — a physical effect that depends on bond angle orientation and crystal structure — its prior observation and use in aragonite, calcite, and vaterite minerals (DeVol et al., 2014) predicts that it also works for dolomite, as demonstrated here for the first time.

PIC mapping reveals that this ooid, like most ooids, is comprised of an outer cortex which formed around an inner nucleus (Fig. 3) (Anderson et al., 2020). Here, the cortex is dominantly comprised of small acicular (needle-shaped) crystals, while crystals in the nucleus are generally larger and equant. We highlight six observations of the outer cortex that together describe a novel dolomite crystal fabric: (1) Individual dolomite crystals are

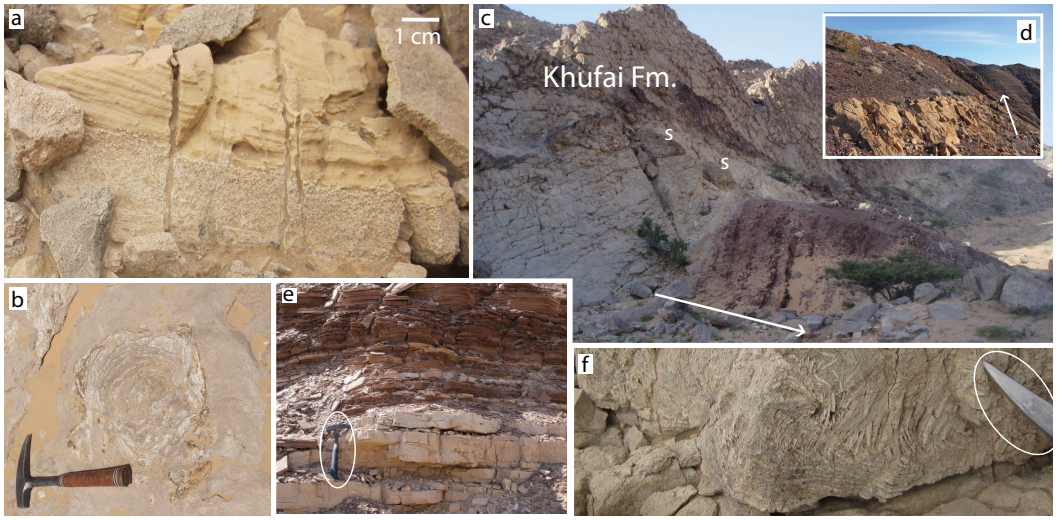

Figure 1. Field photos of the Khufai (Oman) and Johnnie (USA) Formations. **a:** Khufai oolite overlain by cross-stratified, upward fining dolostone. **b:** Cross-section of a stromatolite within the Khufai oolite (plan view). Hammer for scale. **c:** Khufai Formation and overlying red silts of the Shuram Formation, as exposed in Mukhaibah Dome (see (Bergmann et al., 2018; Osburn et al., 2014)). Arrow points to stratigraphic up, 's' denote stromatolitic bioherms within Khufai oolite. **d:** The Khufai-equivalent Johnnie oolite (Death Valley, USA) is also overlain by red silts. Arrow points to stratigraphic up. **e:** Detailed view of the Khufai-to-Shuram gradational transition, Mukhaibah Dome, Oman. Hammer for scale. **f:** Rip-up clasts in stromatolitic facies within Khufai oolite. Hammer pick for scale.

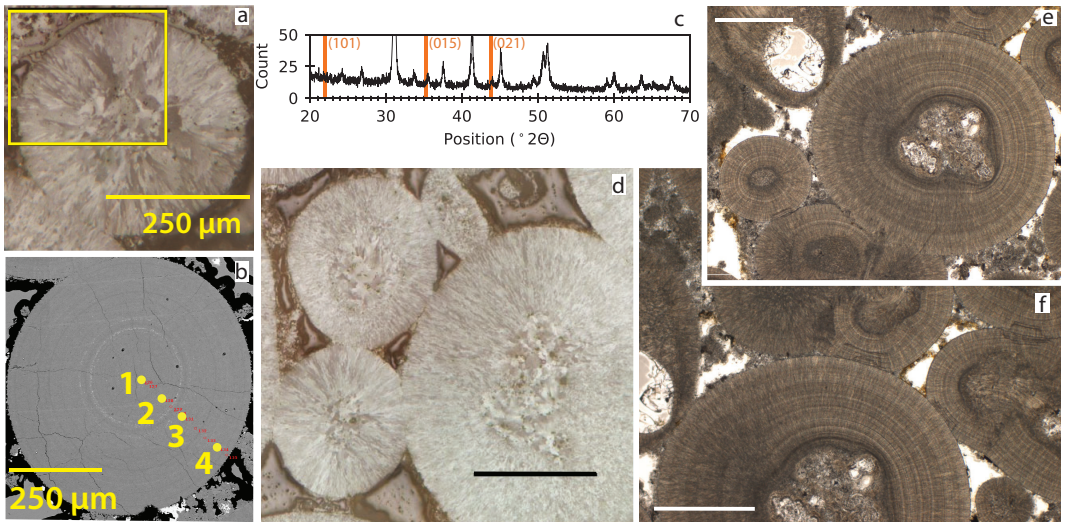

Figure 2. Petrographic images and mineralogy of the Khufai Formation oolite. **a:** Reflected light image. Yellow boxed region was PIC-mapped at 20µm resolution (shown in Figure 3a). **b:** Locations of electron probe micro analysis in a representative ooid within the Khufai oolite. CaO/MgO ratios in spots 1-4 are 21.8/13.2, 21.9/13.1, 22.3/12.7, and 21.8/13.0, respectively. **c:** XRD spectrum of the same oolite. Orange lines indicate dolomite ordering peaks (Kaczmarek et al., 2017). **d:** Reflected light image from the same hand sample as **a**. **e, f:** Thin section images of other ooids from the same bed in the uppermost Khufai Fm. Ooids in **d, e, f** all show the same novel dolomite crystal structure we observe and describe in detail for the ooid in **a** and Figure 3. Scale bars are 500µm unless otherwise noted.

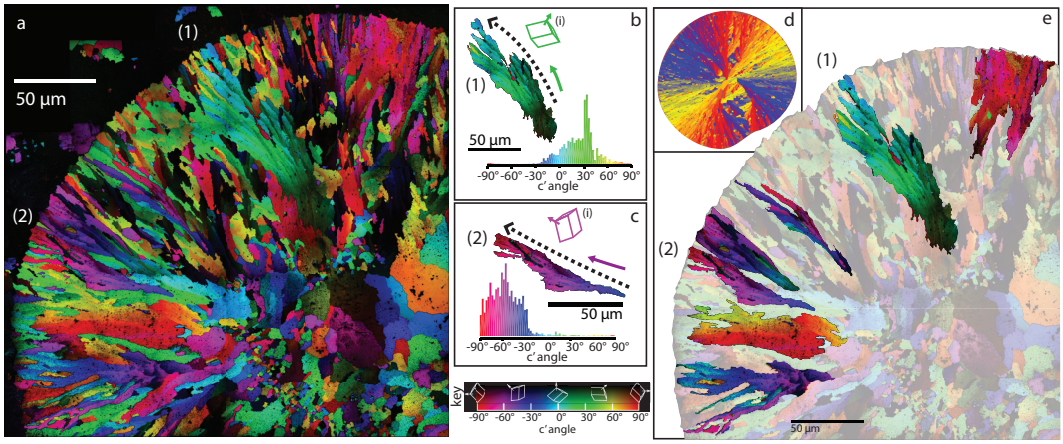

Figure 3. Crystal orientation maps of a fabric-retentive, Ediacaran, dolomitic ooid. **a:** Polarization-dependent Imaging Contrast (PIC) map of the upper quadrant of the ooid shown in Fig. 2a. Each colored region corresponds to one crystal. Colors and brightness represent in-plane (c'-axis) and out-of-plane orientations, respectively, as depicted by the dolomite rhombs and color bar in (labelled "key"). **b, c:** Two bundles of similarly-oriented crystals extracted from the PIC map in **a**, **e** (labeled (1), (2)). Histograms of pixel colors within each bundle show that all crystals within each bundle are similarly oriented. In each case, bundle elongation (dashed lines) and crystal length (solid arrows) are cooriented. Mode crystal orientation for each bundle is depicted by the sketched dolomite rhombs ((i), colored accordingly). The purple bundle, (2), is length-fast; the green bundle, (1), is length-slow. **d:** A modeled spherulitic form (Hendler et al., 2015) resembles the PIC map in A, including plumose bundles, abrupt misorientations, and bundles that terminate at the edge of the form. **e:** Highlighted view of some of the plumose, quasi-spherulitic bundles of similarly-oriented crystals observed in **a.**

small ($\sim$ 2μm by 15μm), acicular, radial, and non-planar (Sibley & Gregg, 1987). (2) Some crystals are grouped into bundles of similarly-oriented crystals (Fig. 3b, c, e). (3) While crystals within each bundle maintain similar orientations (Fig. 3), the optical characteristics of crystals differ between bundles: some are length-fast, with the c-axes pointing along the same vector as the bundle (purple, Fig. 3c) while others are length-slow, with the c-axes pointing perpendicular to the bundle orientation (green, Fig. 3b). (4) Bundles have a curved, plumose morphology that become more expansive towards the edge of the ooid. (5) Most plumose spherulitic bundles terminate at the curved outer edge of the ooid. (6) Textbook Mg:Ca ratios from EPMA (Fig. 2b) and the presence of the (015) and (021) ordering peaks (Kaczmarek et al., 2017) in the XRD spectrum (Fig. 2c) indicate that this ooid is comprised of stoichiometric, ordered dolomite: Ca and Mg are present in equal parts within the carbonate lattice within coherent cation-specific planes.

This combination of features is not completely described by any one of the literature-derived models for fabric-retentive dolomite detailed above, but has some similarities to each. The mimetic replacement model is supported by the EMPA and XRD results and the observed small crystal size, but our ooid's crystals are not rhombohedral. The primary dolomite cement model is supported by this ooid's acicular crystals that form fan-like bundles, but unlike published length-slow examples (Hood et al., 2011; Hood & Wallace, 2018), ooid crystal bundles are variably length-slow and length-fast. The primary protodolomite model is supported by the space filling, radial, elongate crystals arranged in plumose bundles, which show many similarities to documented protodolomite (Rodriguez-Blanco et al., 2015), microbially-mediated (Vasconcelos et al., 1995), and modeled (Hendler et al., 2015) (see Fig 3d) spherulites. Yet, true spherulites always have straight crystals with length-fast orientations, like in plumose spherulite bundles observed in coral skeletons using PIC mapping (Sun et al., 2017). Thus the curved crystals and bundles, variable length-slow and length-fast crystal orientations and the stoichiometric, ordered composition are together inconsistent with the protodolomite model (Rodriguez-Blanco et al., 2015). The spherulite-like crystal bundle morphology we observe – including the consistent optical characteristics of individuals bundles and their plumose geometry – along with the preponderance of bundle terminations at the ooid edge, imply the plumose bundles (e.g. Fig. 3e) grew synchronously during ooid formation.

Our observations show this ooid has the most in common with spherulitic protodolomite and Neoproterozoic dolomite cements: both primary precipitates. However, the variably length-slow and -fast, curved, plumose bundles described here present a novel dolomite crystal morphology. We thus suggest this ooid represents a new crystal fabric formed by primary precipitation of dolomite from seawater.

3.1 Implications for Precambrian environments

With the above evidence that this ooid grew as primary dolomite, it is important to consider its broader depositional context in the ca. 574 Ma Khufai Formation and to use this geologic context to infer the environmental conditions in which this ooid formed. Field sedimentological observations show our ooid is sampled from a cross-stratified ooid-intraclast grainstone deposited in a high-energy, shallow marine setting (Osburn et al., 2014), 1. As stated above, this oolite was deposited at the onset of the Shuram excursion; $\delta^{13}C_{\mathrm{VPDB}}$, $\delta^{18}O_{\mathrm{VPDB}}$, and the carbonate clumped isotope temperature ($T_{\Delta_{47}}$) of the same sample we PIC mapped are -2.8, -7.8, and 66±23°C (2 S.E.), respectively (see Table 3, sample MD6 258.6 in (Bergmann et al., 2018)). Sulfur isotope values measured at the same interval are highly variable, falling "dramatically" from a peak of $\delta^{34}S_{\mathrm{CAS}} = 35$ at the onset of the Shuram excursion (Osburn et al., 2015). To further evaluate our petrographic observation-based hypothesis that this ooid represents primary dolomite precipitation and to further constrain the properties of this ca. 574 Ma shallow marine environment, we can turn to the few modern dolomite analogues that exist and ask whether the Khufai Formation could represent a similar depositional environment.

In the modern, dolomite does form in shallow water environments under specific, localized conditions often in lagoons, sabkha, or lake settings. For example, in the Coorong lakes of South Australia, fine grained (<1 μm - 20μm), spherulitic dolomite precipitates during the hottest, most evaporitic portion of the year in high-salinity, high pH, high [Mg^{2+}] settings dominated by sulfate-reducing bacteria (Wacey et al., 2007). Calculated dolomite precipitation temperatures (from $\delta^{18}O$) fall between ∼40 and ∼90°C, depending on sample location and $\delta^{18}O$ temperature calibration (see Figure 9 in (Wacey et al., 2007)) and $\delta^{34}S_{V-CDT}$ measured on lakewater precipitates varies between 25 and 30. In Lagoa Vermelha, Brazil, Ca-rich dolomite with depleted $\delta^{13}C$ (-7.49 to -8.98) forms in anoxic, hypersaline conditions dominated by sulfate-reducing bacteria at the sediment-water interface (Vasconcelos & McKenzie, 1997; Vasconcelos et al., 2006). This primary precipitated dolomite then "ages" in the anoxic sediment column (<1m depth) to a more stoichiometric, ordered form (Vasconcelos & McKenzie, 1997; Vasconcelos et al., 2006).

While neither the Coorong Lakes nor Lagoa Vermelha dolomites can be taken as perfect analogues for the Khufai Formation (no ooids have been found in either location), the geochemical and physical properties of these exemplary modern locales have much in common with the Khufai oolite, lending support to our hypothesis that the ooid studied here formed via primary precipitation from solution. The presence of sulfur-reducing bacteria is thought to be critical to dolomite formation in both modern examples, and has been identified in laboratory studies as a potential mechanism (through the production of dissolved sulfide

and subsequent disruption of Mg^{2+}-water complexes) for the precipitation of dolomite in the geologic record (see, for example, (Zhang et al., 2012)). We suggest that warm water temperatures, periodically evaporitic conditions, the presence of dissolved sulfide and sulfate-reducing bacteria, and a source of Mg^{2+} ions (Given & Wilkinson, 1987; von der Borch et al., 1975), could have combined to create a shallow marine environment conducive to the precipitation of dolomite in the late Ediacaran period. Similarities in ooid petrography and stratigraphy between the Shuram-aged successions in Death Valley (Bergmann et al., 2011; Corsetti et al., 2006; Tucker, 1982) and Oman ((Bergmann et al., 2018; Osburn et al., 2014) and this study) suggest that these favorable dolomite conditions may have been widespread across shallow marine platforms around 574 Ma.

Appendix A Materials and methods

A1 Sample preparation

All of the analyses described here were conducted on parts of one hand sample (ca. 10 by 10 cm) of oolite collected by K. Bergmann from the upper Khufai Formation, Sultanate of Oman (MD6 258.6, see Bergmann et al. (2018); Osburn et al. (2014)). To prepare for PIC mapping, the sample was cut down to a $4mm^3$ cube, polished and coated with 1nm of Pt following (Sun et al., 2017). A second cut of the sample was thin sectioned, finished with a microprobe-quality polish to 0.25μm and carbon coated for electron probe spot analysis (Fig. 2b). For X-ray diffraction (Fig. 2c), a third section of the oolite sample was powdered using a drill press (Bergmann et al., 2018).

A2 Polarization-dependent Imaging Contrast (PIC) Mapping

We collected the data displayed in the PIC map in Fig. 3 on beamline 11.0.1.1 at the Advanced Light Source, Lawrence Berkeley National Laboratory, using X-ray PhotoEmission Electron spectroMicroscopy (X-PEEM). The polished sample was mounted such that incident X-ray beams hit the sample at a 60° incident angle. Working at a fixed photon energy of 534 eV (π^* peak in carbonate oxygen K-edge spectra), the linear polarization was rotated at the undulator source from 0° to 90° at 5° increments. Each of the resulting 19 images (one at each 5° increment) were stacked and analyzed using GG Macros (see (Sun et al., 2017)). In each pixel of the stack, the intensity (I) vs. polarization angle (χ) curve was fitted using a cosine-squared function: $I = a + bcos^2(\chi - c')$ (Malus's law) with three fit parameters – a, b and c' – where c' is the in-plane and b/a the out-of-plane angle of the crystal c-axis orientation, displayed by hue and brightness as shown by the color legend in Fig. 3 (Gilbert et al., 2011; DeVol et al., 2014). This process was repeated for a series of 56 by 56 μm areas with 56nm pixels partly overlapping to cover the entire quadrant of the ooid

outlined in Fig. 2a. The ~ 50 images were then stitched together using Adobe Photoshop CC 2017 to produce the PIC map shown in Fig. 3a. Together, the hue and brightness of each pixel in a PIC map completely describe the three-dimensional orientation of a crystal's c-axis at the same coordinates as the pixel.

A3 X-ray diffraction (XRD)

Oolite powder was analyzed on the PANalytical X'Pert Pro in the Material Science Department at the California Institute of Technology by (Bergmann et al., 2018). Scans were run from 5-70° 2θ with a step size of 0.008 and a scan step time of 10.16 s. A Cu anode was used at 45 kV and 40 mA. A zero-background silicon plate was used for all measurements. Mineralogical phases were initially identified using the X'Pert Highscore IDMin function in Jade.

A4 Electron probe microanalysis (EPMA)

Electron probe spot analyses, shown in Fig. 2b, were taken using a JEOL JXA-8200 Electron Microprobe at the California Institute of Technology with an accelerating voltage of 15 kV, beam current of 20nA, and beam size of 1 μm. Calcite and dolomite standards were used to calibrate the Ca and Mg measurements, respectively. Average detection limits for Ca and Mg were 177 ppm and 283 ppm, respectively. The CITZAF method was used for matrix correction.

Acknowledgments

JW thanks C. Sun for help with sample preparation at UW-Madison and PIC mapping at LBNL. KDB thanks M. Osburn, J. Grotzinger and W. Fischer for field and laboratory support. oolite, and C. Ma for EPMA assistance. PG acknowledges 80% support from the U.S. DOE, Office of Science, Office of Basic Energy Sciences, Chemical Sciences, Geosciences, and Biosciences Division, under Award DE-FG02-07ER15899, and 20% support from NSF grant DMR-1603192. PEEM experiments were done at the Advanced Light Source, supported by beamline scientist R. Chopdekar, and the Director, Office of Science, Office of Basic Energy Sciences, US DOE under Contract No. DE-AC02-05CH11231. Additional funding was provided by the Packard Foundation to KDB. All data (high-resolutiono PIC map, XRD peaks, and EPMA spot analyses) are stored in a github repository (https://github.com/juliawilcots/synchrotron-paper-data). Geochemical data are referenced in the text. The authors report no conflicts of interest.

References

Anderson, N. T., Cowan, C. A., & Bergmann, K. D. (2020). A case for the growth of ancient ooids within the sediment pile. *Journal of Sedimentary Research*, *90*(8), 843–854.

Bergmann, K. D., Al Balushi, S. A. K., Mackey, T. J., Grotzinger, J. P., & Eiler, J. M. (2018). A 600-million-year carbonate clumped-isotope record from the Sultanate of Oman. *Journal of Sedimentary Research*, *88*(August), 960–979.

Bergmann, K. D., Zentmyer, R. A., & Fischer, W. W. (2011). The stratigraphic expression of a large negative carbon isotope excursion from the Ediacaran Johnnie Formation, Death Valley. *Precambrian Research*, *188*(1-4), 45–56.

Cantine, M. D., Knoll, A. H., & Bergmann, K. D. (2020). Carbonates before skeletons: A database approach. *Earth-Science Reviews*, *201*, 103065.

Corsetti, F. A., Kidder, D. L., & Marenco, P. J. (2006). Trends in oolite dolomitization across the Neoproterozoic-Cambrian boundary: A case study from Death Valley, California. *Sedimentary Geology*, *191*(3-4), 135–150. doi: 10.1016/j.sedgeo.2006.03.021

Derry, L. A. (2010). A burial diagenesis origin for the Ediacaran Shuram–Wonoka carbon isotope anomaly. *Earth and Planetary Science Letters*, *294*(1-2), 152–162.

DeVol, R. T., Metzler, R. A., Kabalah-Amitai, L., Pokroy, B., Politi, Y., Gal, A., ... others (2014). Oxygen spectroscopy and polarization-dependent imaging contrast (pic)-mapping of calcium carbonate minerals and biominerals. *The Journal of Physical Chemistry B*, *118*(28), 8449–8457.

Gilbert, P. U. P. A., Young, A., & Coppersmith, S. N. (2011). Measurement of c-axis angular orientation in calcite (CaCO3) nanocrystals using X-ray absorption spectroscopy. *Proceedings of the National Academy of Sciences*, *108*(28), 11350–11355. doi: 10.1073/pnas.1107917108

Given, R. K., & Wilkinson, B. H. (1987). Dolomite abundance and stratigraphic age; constraints on rates and mechanisms of Phanerozoic dolostone formation. *Journal of Sedimentary Research*, *57*(6), 1068–1078.

Grotzinger, J. P., Fike, D. A., & Fischer, W. W. (2011). Enigmatic origin of the largest-known carbon isotope excursion in Earth's history. *Nature Geoscience*, *4*(5), 285–292.

Hendler, N., Mentovich, E., Korbuly, B., Pusztai, T., Gránásy, L., & Richter, S. (2015). Growth control of peptide-nanotube spherulitic films: Experiments and simulations. *Nano Research*, *8*(11), 3630–3638.

Hood, A. v. S., & Wallace, M. W. (2018). Neoproterozoic marine carbonates and their paleoceanographic significance. *Global and Planetary Change*, *160*(November 2017), 28–45. Retrieved from `https://doi.org/10.1016/j.gloplacha.2017.11.006` doi: 10.1016/j.gloplacha.2017.11.006

Hood, A. v. S., Wallace, M. W., & Drysdale, R. N. (2011). Neoproterozoic aragonite-

dolomite seas? Widespread marine dolomite precipitation in Cryogenian reef complexes. *Geology*, *39*(9), 871–874. doi: 10.1130/G32119.1

Kaczmarek, S. E., Gregg, J. M., Bish, D. L., Machel, H. G., Fouke, B. W., MacNeil, A., ... others (2017). Dolomite, very-high magnesium calcite, and microbes: implications for the microbial model of dolomitization. In *Characterization and modeling of carbonates–mountjoy symposium* (Vol. 1, pp. 7–20).

Knoll, A., & Swett, K. (1990). Carbonate deposition during the late Proterozoic Era: an example from Spitsbergen. *American Journal of Science*, *290*, 104–132.

Osburn, M. R., Grotzinger, J. P., & Bergmann, K. D. (2014). Evolution of a middle Ediacaran carbonate ramp: Khufai Formation, Sultanate of Oman. *AAPG Bulletin*, *98*(8), 1631–1667. doi: 10.1306/07291312140

Osburn, M. R., Owens, J., Bergmann, K. D., Lyons, T. W., & Grotzinger, J. P. (2015). Dynamic changes in sulfate sulfur isotopes preceding the Ediacaran Shuram Excursion. *Geochimica et Cosmochimica Acta*, *170*, 204–224.

Rodriguez-Blanco, J. D., Shaw, S., & Benning, L. G. (2015). A route for the direct crystallization of dolomite. *American Mineralogist*, *100*(5-6), 1172–1181. doi: 10.2138/am-2015-4963

Sandberg, P. A. (1975). New interpretations of Great Salt Lake ooids and of ancient non-skeletal carbonate mineralogy. *Sedimentology*, *22*, 497–537.

Sibley, D. F., & Gregg, J. M. (1987). Classification of dolomite rock textures. *Journal of Sedimentary Research*, *57*(6), 967–975.

Sun, C. Y., Marcus, M. A., Frazier, M. J., Giuffre, A. J., Mass, T., & Gilbert, P. U. (2017). Spherulitic Growth of Coral Skeletons and Synthetic Aragonite: Nature's Three-Dimensional Printing. *ACS Nano*, *11*(7), 6612–6622. doi: 10.1021/acsnano.7b00127

Tucker, M. E. (1982). Precambrian dolomites: Petrographic and isotopic evidence that they differ from Phanerozoic dolomites. *Geology*, *10*(January), 7–12.

Tucker, M. E. (1983). Diagenesis, geochemistry, and origin of a Precambrian dolomite; the Beck Spring Dolomite of eastern California. *Journal of Sedimentary Research*, *53*(4), 1097–1119.

Vasconcelos, C., & McKenzie, J. A. (1997). Microbial mediation of modern dolomite precipitation and diagenesis under anoxic conditions (lagoa vermelha, rio de janeiro, brazil). *Journal of sedimentary Research*, *67*(3), 378–390.

Vasconcelos, C., McKenzie, J. A., Bernasconi, S., Grujic, D., & Tiens, A. J. (1995). Microbial mediation as a possible mechanism for natural dolomite formation at low temperatures. *Nature*, *377*(6546), 220–222.

Vasconcelos, C., Warthmann, R., McKenzie, J. A., Visscher, P. T., Bittermann, A. G., &

van Lith, Y. (2006). Lithifying microbial mats in Lagoa Vermelha, Brazil: modern Precambrian relics? *Sedimentary Geology*, *185*(3-4), 175–183.

von der Borch, C. C., Lock, D. E., & Schwebel, D. (1975). Ground-water formation of dolomite in the Coorong region of South Australia. *Geology*, *3*(5), 283–285.

Wacey, D., Wright, D. T., & Boyce, A. J. (2007). A stable isotope study of microbial dolomite formation in the Coorong Region, South Australia. *Chemical Geology*, *244*(1-2), 155–174.

Zempolich, W. G., & Baker, P. A. (1993). Experimental and natural mimetic dolomitization of aragonite ooids. *Journal of Sedimentary Research*, *63*(4), 596–606.

Zhang, F., Xu, H., Konishi, H., Kemp, J. M., Roden, E. E., & Shen, Z. (2012). Dissolved sulfide-catalyzed precipitation of disordered dolomite: Implications for the formation mechanism of sedimentary dolomite. *Geochimica et Cosmochimica Acta*, *97*, 148–165.